CCM-80-4

Center for Composite Materials

A MODEL OF PASSIVE THERMAL NONDESTRUCTIVE EVALUATION OF COMPOSITE LAMINATES

JOHN A. CHARLES
DALE W. WILSON

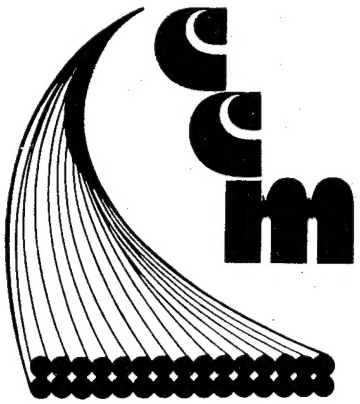

College of Engineering
University of Delaware
Newark, Delaware

*MSG DI4 DROLS PROCESSING - LAST INPUT IGNORED

*MSG DI4 DROLS PROCESSING-LAST INPUT IGNORED

-- 1 OF 2
-- ***DTIC DOES NOT HAVE THIS ITEM***
-- 1 - AD NUMBER: D430432
-- 5 - CORPORATE AUTHOR: DELAWARE UNIV NEWARK CENTER FOR COMPOSITE
-- MATERIALS
-- 6 - UNCLASSIFIED TITLE: A MODEL OF PASSIVE THERMAL NONDESTRUCTIVE
-- EVALUATION OF COMPOSITE LAMINATES,
--10 - PERSONAL AUTHORS: CHARLES,J. A. ;WILSON,D. W. ;
--11 - REPORT DATE: MAY , 1980
--12 - PAGINATION: 32P
--14 - REPORT NUMBER: CCM-80-4
--20 - REPORT CLASSIFICATION: UNCLASSIFIED
--22 - LIMITATIONS (ALPHA): APPROVED FOR PUBLIC RELEASE; DISTRIBUTION
-- UNLIMITED. AVAILABILITY: CENTER FOR COMPOSITE MATERIALS, UNIVERSITY
-- OF DELAWARE, NEWARK, DE. 19711.
--33 - LIMITATION CODES: 1

-- END Y FOR NEXT ACCESSION END

Alt-Z FOR HELP3 ANSI 3 HDX 3 3 LOG CLOSED 3 PRINT OFF 3 PARITY

A MODEL OF PASSIVE THERMAL NONDESTRUCTIVE EVALUATION OF COMPOSITE LAMINATES

John A. Charles*

Dale W. Wilson**

* Assistant Professor, Department of Mechanical Engineering, The Ohio State University, Columbus, Ohio 43210

** Research Associate II, Center for Composite Materials, University of Delaware, Newark, Delaware 19711

May 1980

ABSTRACT

A numerical model of passive thermal nondestructive evaluation of composite laminates was developed. This model, based on a transient, three-dimensional, finite difference solution to the heat conduction equations, can be used to characterize in-plane defects in the laminates and to predict the laminate response to the thermal test. The model was experimentally verified using two material systems. A parametric study was then conducted to ascertain which variables were critical to the success of passive thermal NDE, and how flaw resolution might be improved.

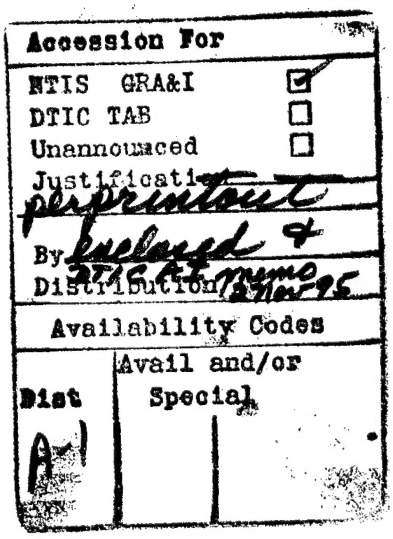

INTRODUCTION

As composite materials become more and more widely accepted for use in structures and machines, the need for quality control and integrity assurance becomes more acute. Therefore, the field of nondestructive evaluation (NDE) takes on increased importance in the development and use of composites. Several NDE techniques are currently available or under investigation for use with composite materials. These include ultrasonic inspection, accoustic emission, holography, x-ray, and more. A relatively new field of study is thermography, or the use of thermal imaging of surface temperature distributions on a composite material to ascertain the integrity of the sub-surface structure.

Thermography received considerable attention as a medical diagnostic tool in the late 1960's [1]. Engineering applications of thermography began to be seen in the 1970's, with energy conservation [2], electronic circuit quality control [3], and material studies each receiving attention. In the area of material evaluation, some initial work was done using an "active" mode of testing in which the material is cyclically stressed while its surface temperatures are monitored thermographically [4-15]. Heat dissipation from hysteretic and other effects led to temperature distributions on the material surface which were related to the stress distributions in the material. In this manner, areas most likely to experience significant damage in service could quickly be located. These

active tests were conducted using both metals and composites. Loading was either by direct fatigue or by vibrational means.

A second mode of thermal testing was also investigated, but received considerably less attention. This mode can be called "passive", since the material does not itself produce the thermal energy, but rather is subjected to heating from an external source [12, 14]. This mode produces images which are transient in nature and therefore harder to capture thermographically. However, the possible advantages of this method over active testing have led to further interest in the development of a viable passive thermal NDE technique. Of primary importance is the feature that passive testing does not subject the material to stressing, other than that caused by thermal gradients, which are small. The elimination of any loading fixtures allows rapid testing of numerous geometries without time-consuming machine adjustments and also makes in-situ testing possible in some applications.

The thermal image developed during passive thermal NDE is the result of a complicated combination of material, defect, and heat source interactions. Usually, the defects to be located are in-plane defects such as delaminations. In this case, heat is applied to the back surface of the laminate while the front surface temperature distribution is observed. The rate of heat application and the mode of heating (contact or radiative) are major parameters. The heat must be conducted from the heated back surface toward the cooler front surface.

Therefore, the conduction heat transfer in the laminate is very important in the process. This conduction heat transfer is complicated by the anisotropic nature of the laminate. The defect, lying between two laminae, serves as a conduction barrier to the flow of heat. It is this restriction of heat flow which eventually produces an image on the front surface of the specimen which implies the presence of the flaw. The degree of conductive resistance is therefore also an important parameter.

In order for passive thermal NDE to progress from a laboratory phenomenon to a useful NDE tool, an understanding of the interactions outlined above is necessary.

The usefulness of appropriate models in characterizing the effects of these interactions on the thermal behavior during test has been discussed by Trezek and Balk [16] for metallic systems. This concept was extended to incorporate the effects of heterogeneity and anisotropy characteristic of composite systems and a model of passive thermal NDE was developed. The model was used to perform a parametric study investigating the effects of the critical parameters on flaw resolution. The model, which was experimentally verified, can be used to predict the behavior of a known flawed laminate under test, or to characterize the thermal properties of a given type of defect. The model is equally useful for any method of thermal imaging, including the two most used methods of liquid crystals and the scanning infrared camera.

THEORY

The problem to be modeled involves the transient flow of heat in a laminated composite material heated suddenly on one surface. The composite is assumed to have an arbitrary number of plies, each with an arbitrary orientation. Furthermore, it is also desired to include an in-plane defect between any two plies in the model. The results of the model are to be in the form of temperature distributions on the front (unheated) surface of the laminate. Thermal gradients on this surface are the most important result from the point of view of NDE, since it is the thermal gradient, and not the temperature itself, which allows thermography to yield any information at all in any test. Once the temperature distribution is calculated, obtaining thermal gradients is quite simple.

Due to the complexity of the problem, including the anisotropic conduction in the composite, it was determined that the best approach to the problem would be through a finite difference solution to the governing differential equation [17],

$$\rho\, C_p \frac{\partial T}{\partial t} = k_x \frac{\partial^2 T}{\partial x^2} + k_y \frac{\partial^2 T}{\partial y^2} + k_z \frac{\partial^2 T}{\partial z^2} \qquad (1)$$

where ρ = net material density

C_p = net material specific heat

T = temperature

$k_{x,y,z}$ = thermal conductivity in x-, y-, and z-directions, respectively.

In the finite difference approach, the body is modeled as an array of nodes, each with an associated volume of material. The governing equation is written for each node, yielding a set of algebraic equations to be solved. For transient problems where initial conditions are known, this solution gives the nodal temperatures at time t+ Δt, where Δt is governed by the numerical stability of the solution.

Since it is desired to model each ply individually, only a small portion of the laminate is modeled. The region selected surrounded the defect projection on the surface. The use of this small section of the laminate is acceptable if the defect does not perturb the heat conduction near the edges of the section, which are assumed to be insulated. It was found that insulated edge conditions were reasonable for the cases studied here.

The remaining boundary conditions imposed on the modeled portion of the material are insulated front and back surfaces. It was assumed that for the short time intervals (on the order of 1 sec.) and the relatively small temperature increases of interest in thermal NDE the errors resulting from neglecting convective and radiative heat losses would not be significant. However, for longer intervals and larger temperature increases, these conditions must be changed. By imposing the insulated surface conditions, considerable simplifications could be realized in the analysis while retaining acceptable accuracy. The final condition imposed is that of a uniform initial material

temperature equal to the ambient temperature.

Heat input to the material can be modeled as either contact or radiative heating. For the case of contact heating, the back surface temperature is elevated to the heating element temperature at time t = 0 and held constant thereafter. For the case of radiative heat input, a heat generation in the back surface nodes is used to simulate actual radiative input. The generation starts at time t = 0, and can be maintained for any desired interval of time. This feature allows for the modeling of pulse heat inputs, such as might be used with a laser heat source.

As mentioned above, it is necessary to model each lamina individually to allow for arbitrary stacking sequences. Therefore, the thermal properties are first obtained in the principal material axis system (1,2,3, where 1 = fiber direction, 2,3 = transverse directions) and then resolved to yield effective properties in the global axis system (x,y,z) of the laminate. The thermal properties are a function of the properties of each of the constituents. In the present case, each lamina is considered a two-component system of fiber and matrix. The density and specific heat of each lamina is then found using the Rule of Mixtures:

$$\rho = \rho_f V_f + \rho_m (1-V_f) \tag{2}$$

$$C_p = C_f V_f + C_m (1-V_f) \tag{3}$$

where V_f = volume fraction of fiber

$(\ )_m$ = matrix properties

$(\ )_f$ = fiber properties

Within each ply, the thermal conductivity in the longitudinal (fiber) direction (k_1) and transverse directions (k_2) may be calculated [18]

$$k_1 = k_f V_f + k_m(1-V_f) \tag{4}$$

$$k_2 = k_m \left[\frac{k_f(1+V_f)+k_m(1-V_f)}{k_f(1-V_f)+k_m(1+V_f)}\right] \tag{5}$$

where k_f = fiber conductivity

k_m = matrix conductivity

Knowing these thermal conductivities, the global (x,y,z) conductivities are easily obtained:

$$\begin{aligned} k_x &= |k_1 \cos\theta| + |k_2 \sin\theta| \\ k_y &= |k_1 \sin\theta| + |k_2 \cos\theta| \\ k_z &= k_2 \end{aligned} \tag{6}$$

where θ = fiber orientation angle with respect to the global x-axis. The properties to be used in the numerical model are those given in Equations (2), (3), and (6).

DESCRIPTION OF DEFECT

The approach described thus far will suffice for modeling an unflawed material, but in the present study an important part of the model addressed the simulation of a defect. It is assumed that a defect, either natural or implanted, in the x-y plane serves as a conduction inhibitor in the z-direction. Hence, to model the defect, the z-direction thermal conductivity

is reduced between two plies over a portion of the modeled section. This introduces the concept of the "Defect Conduction Factor" (DCF), such that

$$kz_{DEFECT} = DCF \cdot k_z \ , \qquad (7)$$

where kz_{DEFECT} represents the z-conductivity at the defect and kz is from Equation (6). The DCF usually varies from 0 to 1.00. For no defect, the DCF = 1.00, while a complete delamination with no physical contact between the plies displays a DCF close to 0.

It is possible to characterize the thermal behavior of defects using only the DCF. Note that since the defects lie between two plies in this model, the x- and y-conductivities will be unaffected. For cases of damaged plies, rather than delaminations, the model must be revised.

NODAL EQUATIONS

Using the thermal properties derived and the concept of the defect conduction factor, it is possible to write the nodal equations for the finite difference. As an example, the nodal equation for all internal nodes are given here. Considering node (i,j,k) and letting

$T_{i,j,k}'$ = nodal temperature at time $t+\Delta t$

$T_{i,j,k}$ = nodal temperature at time t

Δt = time interval.

Then the resulting nodal equation is

$$T_{i,j,k}' = \frac{k_{x_k}}{A}(T_{i-1,j,k}+T_{i+1,j,k}) + \frac{k_{y_k}}{A}(T_{i,j-1,k}+T_{i,j+1,k})$$

$$+ \frac{k_{z_{i,j,k-1}} n^2}{A}(T_{i,j,k-1}) + \frac{k_{z_{i,j,k}} n^2}{A}(T_{i,j,k+1}) \quad (8)$$

$$- \frac{T_{i,j,k}}{A}\left[2(k_{x_h}+k_{y_k}) + n^2(k_{z_{i,j,k-1}}+k_{z_{i,j,k}}) - A\right]$$

where $A = \rho C n^2 dz^2/\Delta t$

n = nodal aspect ratio = $dx/dz = dy/dz$

dz = nodal thickness = ply thickness.

Note that the x- and y-thermal conductivities, which were given by Equation (6) are subscribted $(\ )_k$ indicating that they have a different value for each ply. The z-conductivity must be handled in a different manner since it may change within a given ply due to the presence of a defect. Hence,

$k_{z_{i,j,k-1}}$ = conductivity at node (i,j) in ply (k) governing heat flow from ply (k-1) to ply (k).

$k_{z_{i,j,k}}$ = conductivity at node (i,j) in ply (k) governing heat flow from ply (k) to ply (k+1)

At all (i,j,k) not adjacent to the defect,

$$k_{z_{i,j,k}} = k_t \ . \quad (9)$$

For defects, $k_{z_{i,j,k}} = DCF \cdot k_t$.

Associated with each nodal equation in the finite difference model is a stability criterion. For the case of Equation (8), the final bracketed term must not be less than zero or the 3rd Law of Thermodynamics will be violated [17].

This criterion leads to the selection of a time interval for the solution

$$2(k_{x_k}+k_{y_k}) + n^2(k_{z_{i,j,k-1}}+k_{z_{i,j,k}}) - \frac{\rho Cn^2dz^2}{\Delta t} \geq 0$$

$$\therefore \Delta t \leq \rho Cn^2dz^2/\{2(k_{x_k}+k_{y_k})+n^2(k_{z_{i,j,k-1}}+k_{z_{i,j,k}})\} \qquad (10)$$

In a similar manner, nodal equations such as (8) and stability criteria such as (10) can be derived for each of the different kinds of nodes. In this model, six different types of nodes were used, including interior nodes, top and edge nodes, side and corner nodes and bottom nodes with heat input capabilities. The governing time interval is the smallest one which results from the stability criteria for all nodes. For a typical laminate of graphite/epoxy, with a single ply thickness of 0.140 mm (0.0055 in.), and thermal properties as given in Table 1, the governing time interval is 0.008 seconds. To minimize the total number of equations to be solved in each case (nodal array size times the number of iterations required for the total time of interest) array size of 25 x 25 x (number of plies) was chosen. An illustration of the resulting geometry for a 5-ply laminate is shown in Figure 1. The defect in this case is shown located above ply 2.

NUMERICAL SOLUTION

An interactive computer program was written to perform the simultaneous solutions to the nodal equations. The program input stage first required the specification of material

properties, defect geometry, and laminate stacking sequence. The thermal properties of two common material systems graphite/epoxy and fiberglass/epoxy were included internally. The constituent properties used for these systems are shown in Table 1 and a provision for specification of fiber volume fraction was included. A material system other than that contained internally could also be specified by the user.

Thermal conditions which were input consisted of the specification of ambient temperature and the heat input. Two modes of heat input were modeled; contact heating and radiative heating. For contact heating, only the back surface temperature was specified. For radiative heating, the heat input to the surface and the duration of the input had to be specified.

The defect could be located between any two plies at the user's discretion. Either a "standard" square defect or a defect of arbitrary shape could be specified. The defect conduction factor (DCF) was specified to define the thermal behavior of the defect.

Several output options were available from the program. These included the full upper surface temperature distribution, a "scan" of surface temperatures along the global x-axis, surface temperature gradients at the defect edge, and through-thickness temperature distributions. Temperatures at the center of the back surface were also available for use in model verification.

MODEL VERIFICATION STUDY

In order to verify the accuracy of the finite difference model prior to its use in a parametric study, specimens of graphite/epoxy (Gr/E) and fiberglass/epoxy (G/E) were fabricated and tested under radiant heating. The heat source was an apparatus designed for passive thermal testing using liquid crystals, which irradiated a surface with heat from a bank of light bulbs. The enclosure housing the bulbs was designed to provide a uniform heat input to the surface. The specimens were 8-ply, quasi-isotropic laminates of AS 3501-6 graphite prepreg or 1002 E-glass prepreg, both produced using standard autoclave curing cycles. The laminates were constructed with no defects (i.e., DCF = 1.0), and their integrity was verified by ultrasonic C-scan. Temperatures were measured on the front and back surfaces of the specimens during heating using bondable temperature gages (Micro-Measurements ETG-50B) whose response was recorded on an x-y recorder using a time base.

The numerical model was run for the tested laminates with no defects. By trial and error, the intensity of the radiant heat source was found to be 6941 watts/m^2. Using this heat input and the thermal properties already given in Table 1, excellent agreement between the model and experimental results was obtained. A comparison of the results for Gr/E is shown in Figure 2; that for G/E is shown in Figure 3. The excellent agreement between experiment and theory lend credence to the

model, and give one confidence for its use in a parametric study.

It should be noted that the time interval of interest for passive thermal testing is normally only a few seconds. During this time, the surface temperature gradients on the laminate reach their maximum values and hence yield the greatest resolution in the thermal image. Therefore, only brief time intervals are of prime importance in this study.

An interesting feature of Figures 2 and 3, which is predicted by the model, is the thermal lag between the front and rear surfaces, and the difference in thermal response between the two material systems. The difference in the two systems stems from the much greater thermal conductivity of graphite fibers compared to glass fibers. This gives Gr/E a much higher transverse effective conductivity than G/E, resulting in a more rapid conduction of heat to the front surface in the graphite laminate.

PARAMETRIC STUDY RESULTS AND DISCUSSION

A parametric study of passive thermal NDE of laminates was undertaken to investigate the effects of various parameters on the expected thermal resolution of internal defects. As discussed previously, the temperature gradient across the edge of the defect projection on the viewed surface is of primary concern in passive thermal NDE. Imaging systems can be adjusted to any desired temperature level, so the actual temperatures themselves are only of secondary importance when

resolution is to be maximized. Nevertheless, this temperature level information can be useful in predicting at what levels the gradient is maximized, allowing one to adjust the imaging system accordingly.

The effects of many parameters were studied using the numerical model. Attention here will be given to the effects of heat input mode and strength, flaw depth, size, and thermal properties, and material system. The results are presented in terms of the "edge gradient", which is defined as the temperature gradient across the edge of the defect projection on the upper (viewed) surface. The "peak edge gradient" is the maximum value of the gradient for the time interval considered.

The effect of the mode of thermal input on the edge gradient is shown in Figure 4 for an 8-ply, quasi-isotropic laminate. The flaw being considered is a 7.62 mm square defect with a DCF of 0.50, located above ply 4. The DCF of 0.50 corresponds to the theoretical value of the DCF for an implant of TFE, 0.0025 mm thick, making perfect contact with the plies above and below it. Such implanted defects were used in a related experimental study. The levels of the temperature rises and gradients themselves are not critical in this figure, since they may be altered by changing the intensity of the thermal inputs. However, the relative behavior of the gradients as a function of time is important. Particularly, the radiant heating offers a more gradual decay of the gradient after the peak

gradient is attained. This in effect allows more time at "high" gradient compared to contact heating, which affords a greater chance of obtaining a high-resolution thermal image of the flaw. This feature of radiant heating, and the difficulty of obtaining a truly uniform heat input from contact heating, make the use of radiant heating the desirable mode of thermal input for passive NDE. A possible exception to this argument might occur if a surface were heated by contact with a warm liquid, producing a uniform heat input. Such might be the case in tests of composite pressure vessels or tanks.

The effect of the intensity of the radiant heat input is illustrated in Figure 5. The laminate under consideration is again Gr/E, of the same configuration as the previous case. In this instance, it is seen that the peak gradient varies approximately linearly with heat input to the back surface. However, as the input increases, the time at high gradient decreases. Since the thermal resolution is a function of the maximum gradient, higher heat inputs are recommended for best results, but care must be exercised to avoid missing the image in the brief interval that the gradient is high. The results of this case were used in the related experimental study when poor thermal resolution was initially achieved; an increase in the radiant input intensity recommended from the model resulted in immediate improvements in resolution.

Thus far, only Gr/E laminates have been discussed in the parametric study. The observation made concerning thermal

lag in G/E in the model verification study is also pertinent here. Figure 6 shows the responses of both Gr/E and G/E laminates under radiant heating from a 15775 Watt/m^2. Both laminates were 8-ply with a square defect of 7.62 mm at their mid-planes. For the same heat input, the two material systems display marked different thermal behavior. This of course is expected from comparisons of the thermal properties of the materials in Table 1. The significance of the results in Figure 6, however, is that it can be expected that material systems with lower thermal diffusivity ($k/\rho C_p$) will yield better results under thermal NDE than those with higher diffusivities, such as Gr/E. Moreover, the slower heat transfer in G/E systems retains high edge gradients for a considerably longer time than Gr/E, implying that a higher probability of successful flaw detection exists for G/E laminates. Having observed that G/E systems will yield better NDE results than Gr/E, the remainder of the study will focus on Gr/E laminates.

The defect conduction factor (DCF) can be used to characterize the thermal behavior of a defect. Recall that the DCF is actually a measure of the thermal resistance across the flaw; high values of DCF refer to flaws with little thermal resistance, while a DCF of zero implies a perfect flaw with no conduction between adjacent laminae. As important as this factor is, it is most difficult to determine except for cases of complete delamination. The effect of the DCF on the edge gradient of a square 7.62 mm defect located above ply 4 in an

8-ply Gr/E laminate is shown in Figure 7. The temperature rise indicated is that at the peak gradient. As expected, the selection of the DCF has a pronounced effect on the gradients. Upon further development of experimental techniques in thermal NDE of laminates, information such as that presented in Figure 7 may be used to quantize the behavior of unknown defects from thermal images, leading to conclusions concerning relative flaw severity. It is also seen from Figure 7 that as the DCF decreases, the sensitivity of the imaging system must increase to yield good thermal images.

The effect of defect size on the peak edge gradient is shown in Figure 8. The material system is again 8-ply Gr/E, heated by contact. Both the edge gradient and the time to achieve the peak are influenced by the defect size. For small defects, minor size differences produce significant gradient changes. However, for larger sizes greater than about 12.7 mm the effect of defect size diminishes. Of course, smaller defects yield lower gradients and hence require the use of a thermal imaging system with higher thermal resolution in order to display the gradients. This represents a quantization of the limiting resolution of a given system for flaw detection through passive thermal NDE.

Finally, the effect of flaw depth on the edge gradient is shown in Figure 9. The case illustrated is the 7.62 mm defect in Gr/E. The defect conduction factor is taken to be 0.50. Heat input is radiant. With a DCF of 0.50, the greatest

peak gradient occurs with the defect three plies below the surface rather than only one ply below. This is due to the fact that conduction through the defect is not eliminated in this case, but only retarded. Therefore, heat flows into the volume above the defect both through the defect and from around the defect. Defects deeper than three plies in the laminate show a decrease in the peak edge gradient. The peak edge gradients were found to occur at essentially the same temperature rise, regardless of the flaw depth.

CONCLUSIONS

The sample results shown here are part of a much more comprehensive study of passive thermal NDE conducted in relation to experimental work using liquid crystals. Most of the effects pointed out could be seen using the Gr/E and G/E laminates with implanted flaws. The results of the model, once verified experimentally as shown, could be used to guide the experimental study. Other effects, such as that of stacking sequence in the laminate could be easily studied by using the model developed.

The final goal of this study is to further the state-of-the-art of passive thermal NDE of composite laminates. Without the use of a model such as that presented here, the success of actual tests is largely a matter of "art" or perhaps chance. Using an accurate model of the process, it is possible to predict system responses under test conditions and adjust the thermal imaging system accordingly. Resolution limits can also

be determined for a given imaging system and material/heat source combination. Finally, it should be possible with sufficient experimental data from tests of known defects to establish defect conduction factors for different types of defects (inclusions, full delaminations, partial delaminations, etc.). These results and comparisons with thermal images of unknown defects will allow the quantization of defect types and the determination of their severity. When these aims are achieved, passive thermal NDE of laminates will become more science than art and will be a viable NDE tool for industry.

TABLE 1. MATERIAL PROPERTIES USED IN MODEL

PROPERTY (Units)	GRAPHITE/EPOXY		FIBERGLASS/EPOXY	
	FIBER	MATRIX	FIBER	MATRIX
Density (gm/cm^3)	1.85	1.15	2.50	1.15
Specific Heat (kJ/kg-C)	0.75	1.88	0.79	1.88
Thermal Conductivity (Watt/m-C)	173.07	0.27	10.38	0.16

REFERENCES

1. Karpman, H.L., "Current Status of Thermography", Angiology, 21, pp. 103-109, (Feb. 1970).

2. Marshall, S.J., "Infrared Thermography of Buildings", Cold Regions Research and Engineering Laboratory, Hanover, New Hampshire, AD-A038 447, (March 1977).

3. Leftwich, R.F. and Ordway, G.B., "Optical Thermal Testing - A State of the Art Review", International Journal of Non-destructive Testing, 2, pp. 129-170, (1970).

4. Attermo, R. and Ostberg, G., "Measurements of the Temperature Rise Ahead of a Fatigue Crack", International Journal of Fracture Mechanics, 7(1), pp. 122-124, (March 1971).

5. Reifsnider, K.L. and Williams, R.S., "Determination of Fatigue-related Heat Emission in Composite Materials", Experimental Mechanics, 14(12), pp. 479-485, (Dec. 1974).

6. Marcus, L.A. and Stinchcomb, W.S., "Measurement of Fatigue Damage in Composite Materials", Experimental Mechanics, 15(2) pp. 55-60, (Feb. 1975).

7. Charles, J.A., Appl, F.J., and Francis, J.E., "Using the Scanning Infrared Camera in Experimental Fatigue Studies", Experimental Mechanics, 15(4), pp. 133-138, (April 1975).

8. Salkind, M.J., "Early Detection of Fatigue Damage in Composite Materials", AIAA Paper No. 75-722, presented at the AIAA/ASME/SAE 16th Structures, Structural Dynamics, and Materials Conf., Denver, Colorado, May 1975.

9. Charles, J.A., Appl, F.J., and Francis, J.E., "Fatigue Testing Composites Using Thermography", Proceedings of the 12th Annual Meeting of the Society of Engineering Science, Austin, Texas, pp. 819-828, (Oct. 1975).

10. Nevedunsky, J.J., Lucas, J.J., and Salkind, M.J., "Early Fatigue Damage Detection in Composite Materials", Journal of Composite Materials, 9(4), pp. 394-408, (Oct. 1975).

11. Charles, J.A., Appl, F.J., and Francis, J.E., "Thermographic Determination of Fatigue Damage", Journal of Engineering Materials and Technology, 100(2), pp. 200-203, (April 1978).

12. Charles, J.A., "Use of Liquid Crystals in Detecting Fatigue Damage", SESA Paper No. CR-22, Presented at 1978 SESA Spring Meeting, Wichita, Kansas, May 1978.

13. Whitcomb, J.D., "Thermographic Measurement of Fatigue Damage", NASA Technical Memorandum 78693, (May 1978).

14. Charles, J.A., "Liquid Crystals for Flaw Detection in Composites", Nondestructive Evaluation and Flaw Criticality for Composite Materials, ASTM STP 696, R.B. Pipes, Ed., American Society for Testing and Materials, 1979, pp. 72-82.

15. Henneke, E. G. and Jones, T. S., "Detection of Damage in Composite Materials by Vibrothermography," Nondestructive Evaluation and Flaw Criticality for Composite Materials, ASTM STP 696, R.B. Pipes, Ed., American Society for Testing and Materials, 1979, pp. 83-95.

16. Trezek, G.J. and Balk, S., "Provocative Techniques in Thermal NDT Imaging", Materials Evaluation, Vol. ?, pp. 172-176, (August 1976).

17. Krieth, F., Principles of Heat Transfer, Intext Educational Publishers, New York, pp. 139-216, 1973.

18. Springer, G.S. and Tsai, S.W., "Thermal Conductivities of Unidirectional Materials", Journal of Composite Materials Vol. 1, 1967, pp. 166-173.

5 - PLY LAMINATE :

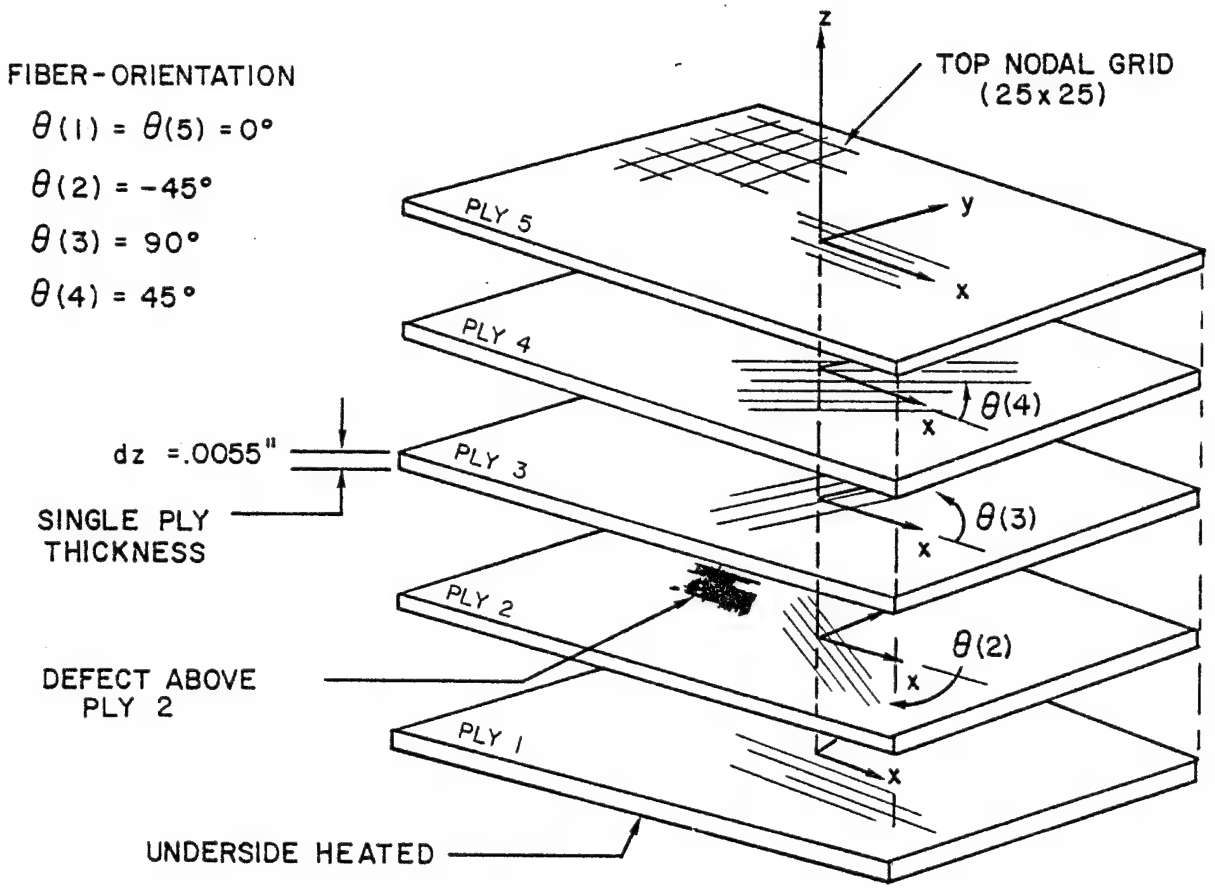

FIGURE 1. TYPICAL LAMINATE GEOMETRY FOR MODEL.

FIGURE 2. COMPARISON OF EXPERIMENTAL AND NUMERICAL RESULTS FOR GRAPHITE / EPOXY.

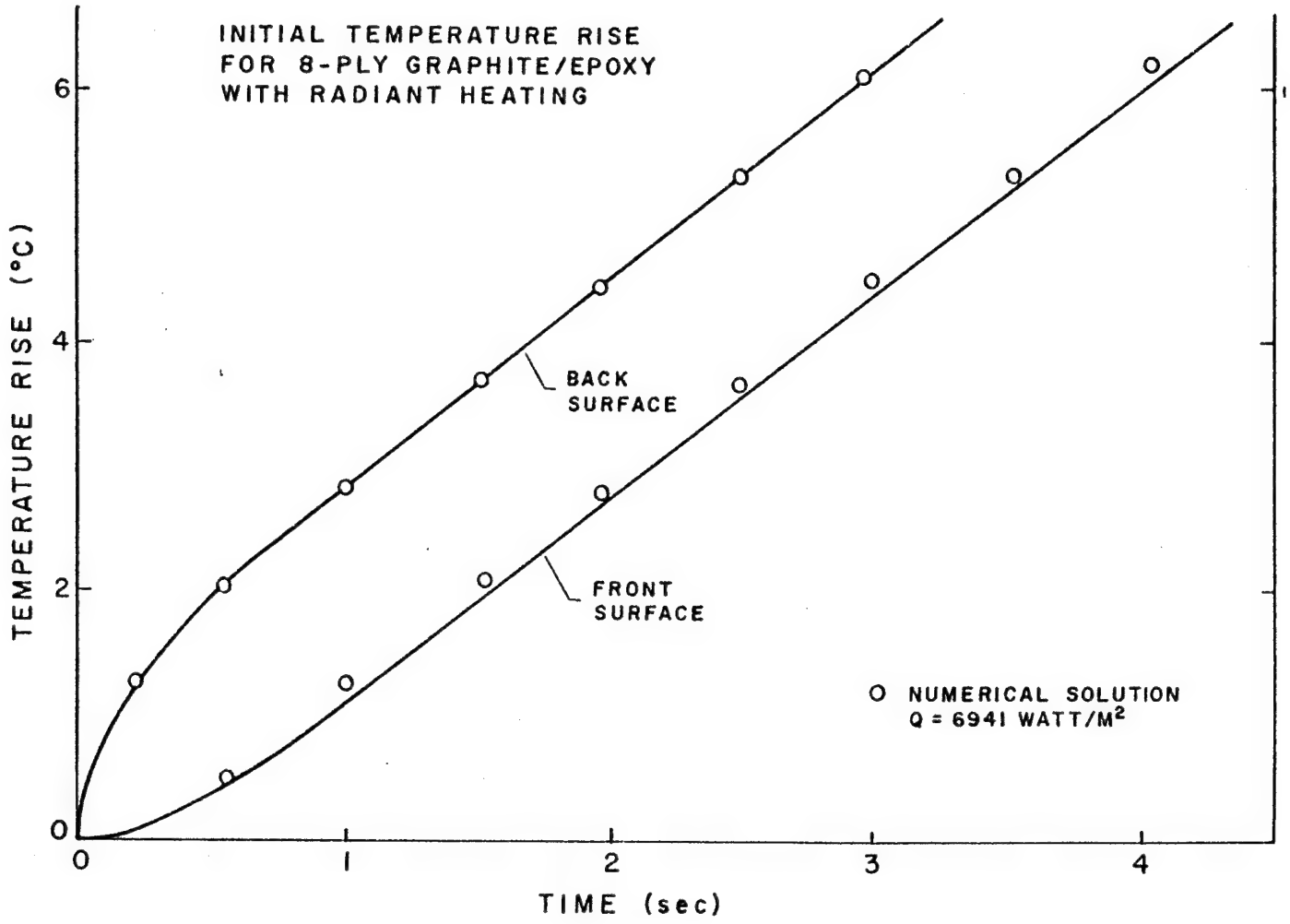

FIGURE 3. COMPARISON OF EXPERIMENTAL AND NUMERICAL RESULTS FOR FIBERGLASS/EPOXY.

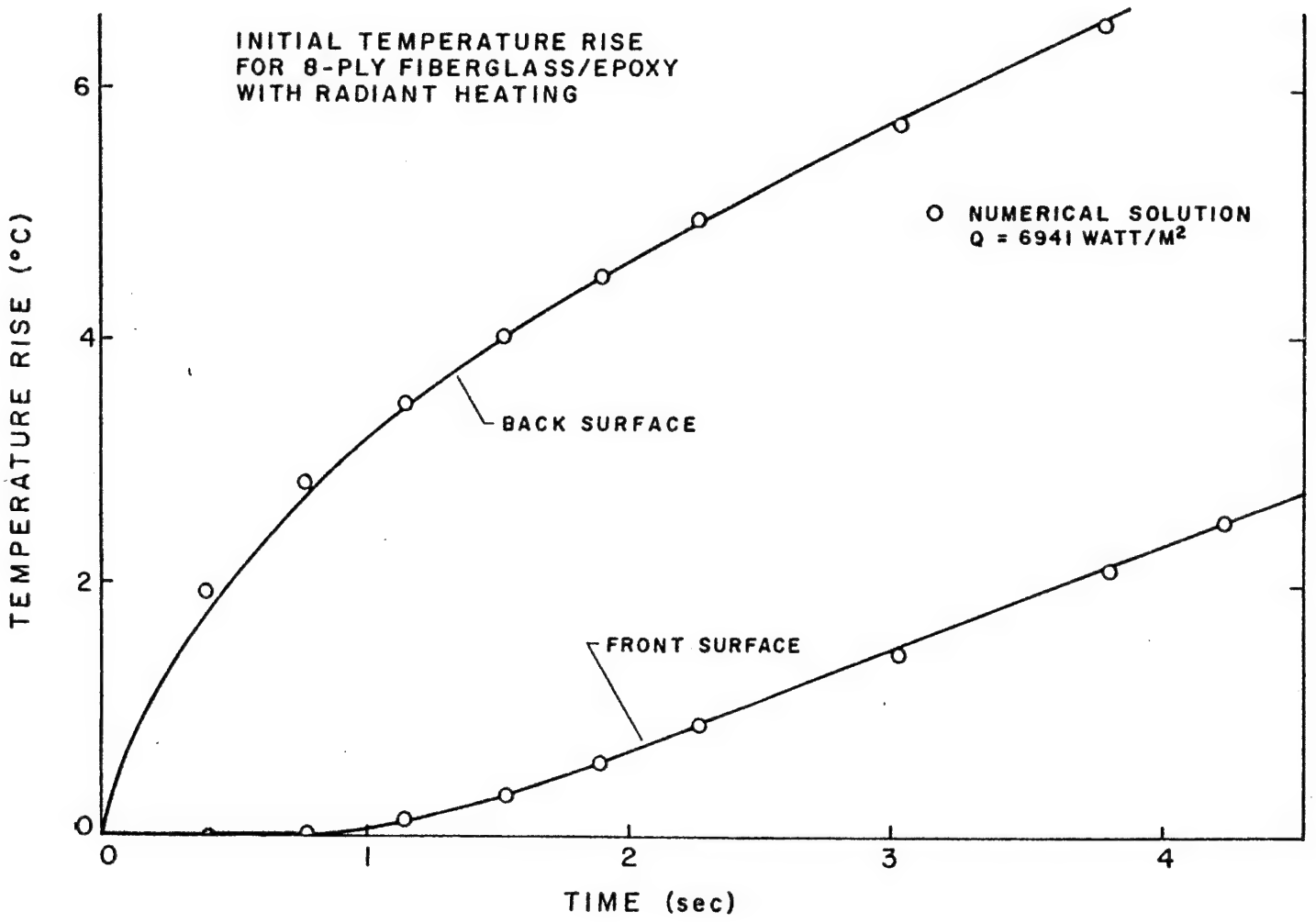

FIGURE 4. EFFECT OF MODE OF THERMAL LOADING ON GRADIENT IN GRAPHITE/EPOXY.

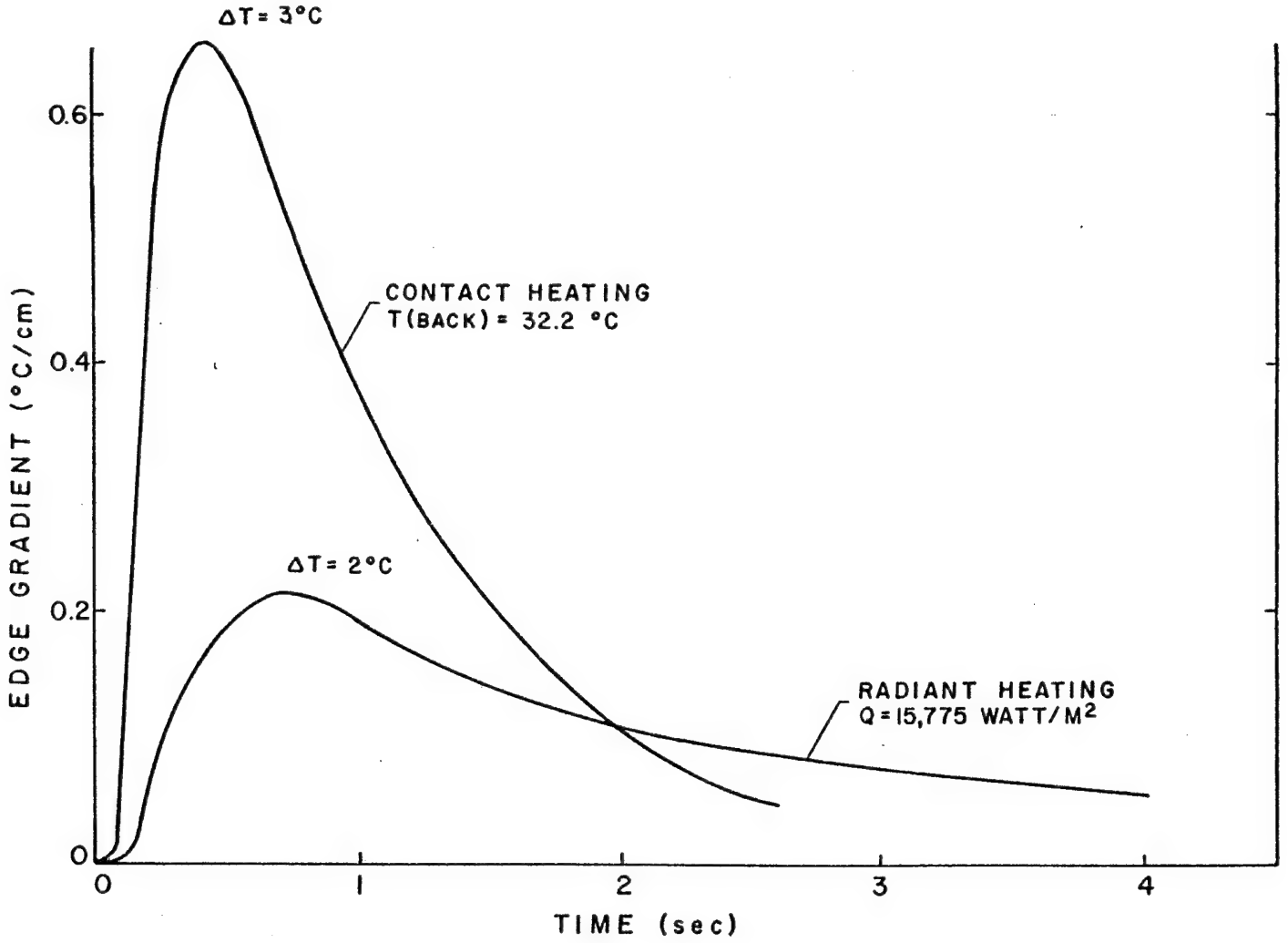

FIGURE 5. EFFECT OF RADIANT INPUT ON GRADIENT IN GRAPHITE/EPOXY.

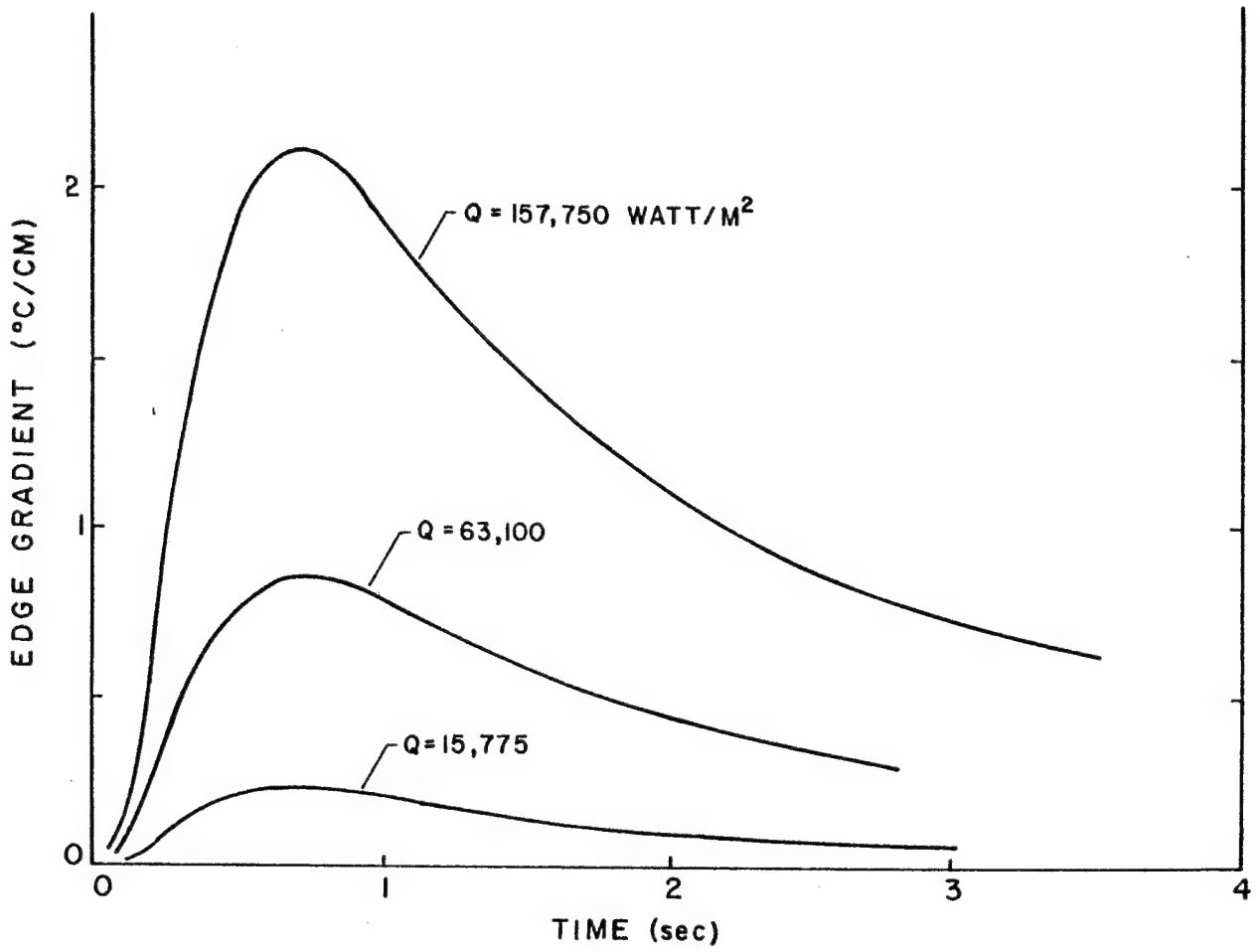

FIGURE 6. EFFECT OF MATERIAL SYSTEM ON GRADIENT AND RESPONSE TIME.

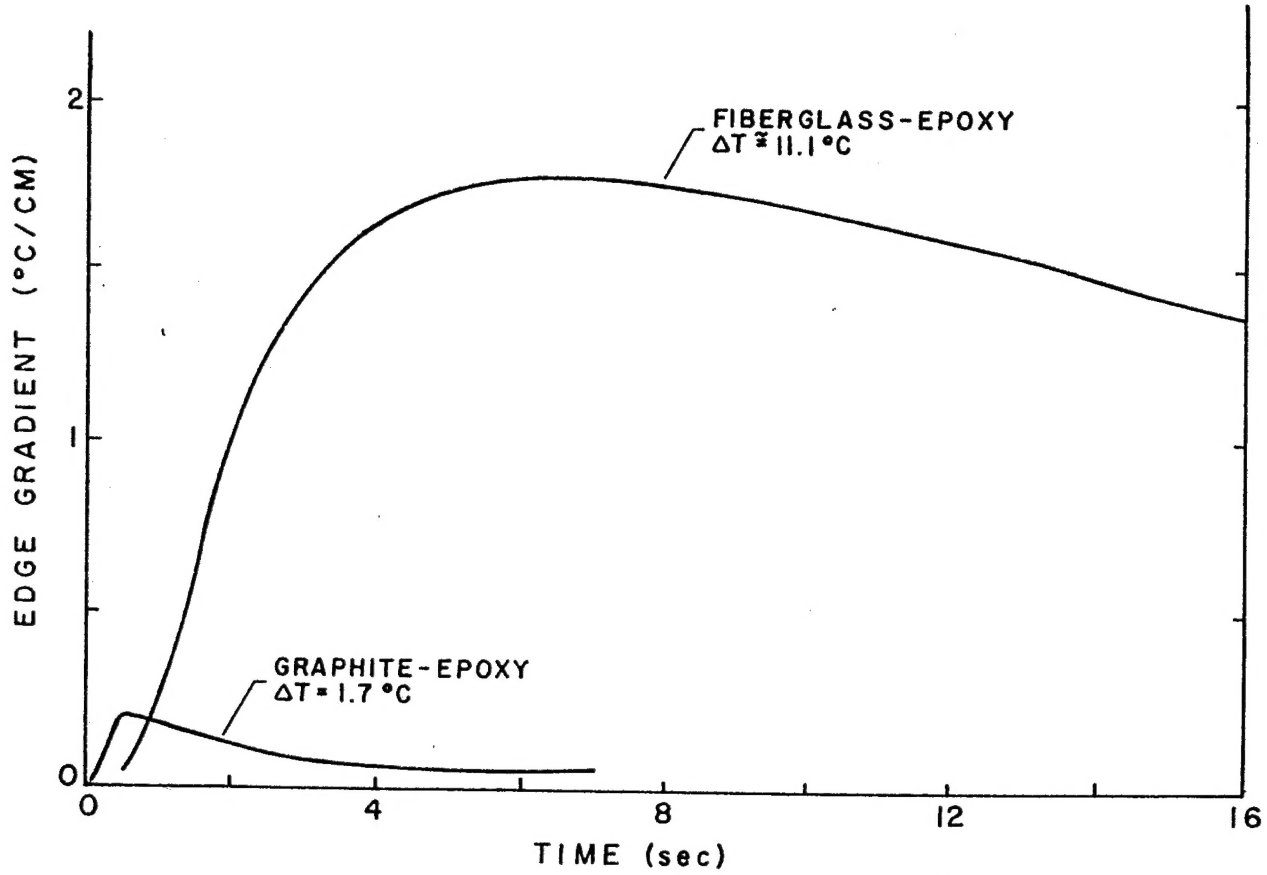

FIGURE 7. EFFECT OF DEFECT CONDUCTION FACTOR ON GRADIENT AND TEMPERATURE RISE IN GRAPHITE/EPOXY.

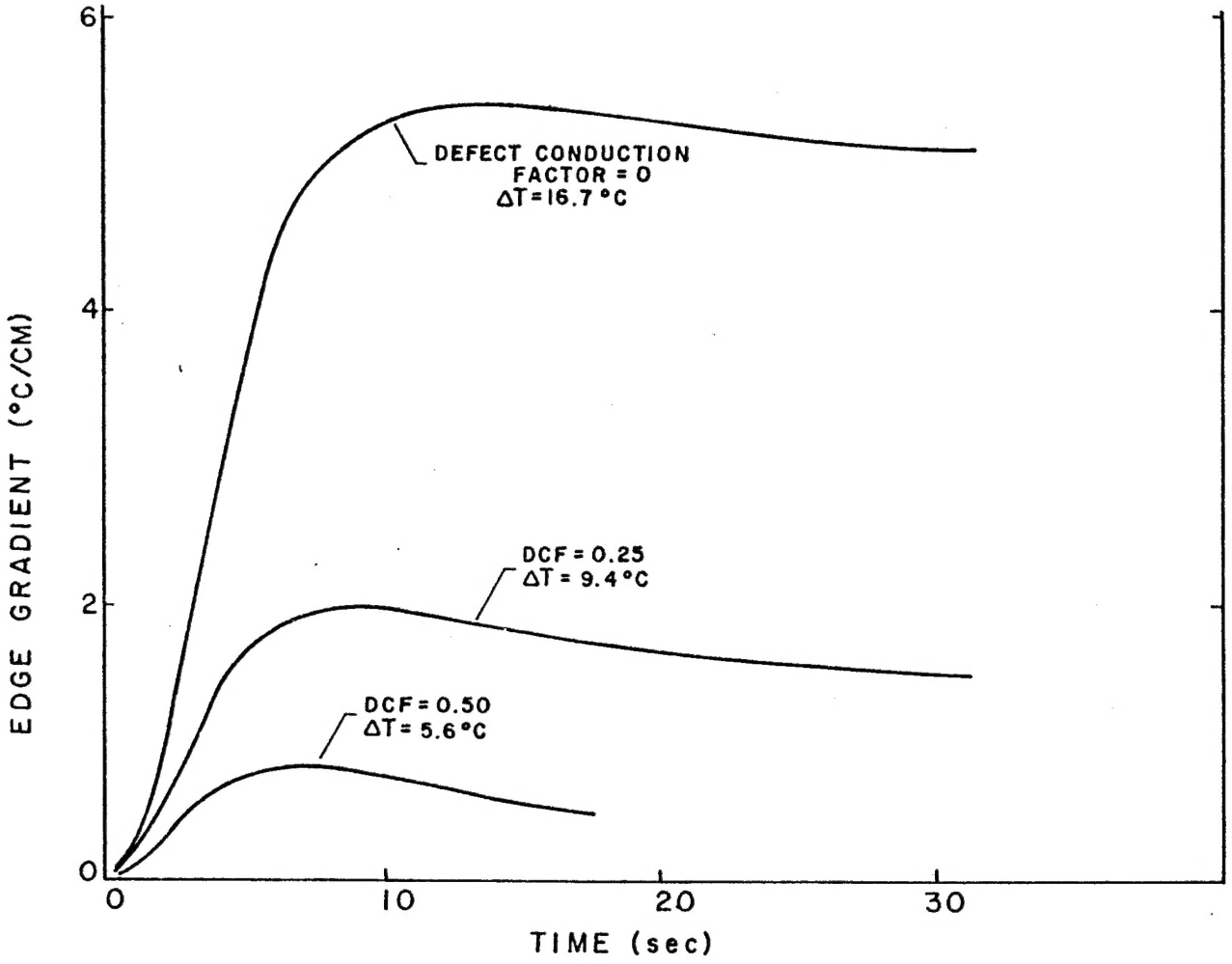

FIGURE 8. EFFECT OF DEFECT SIZE ON MAX. SURFACE GRADIENTS.

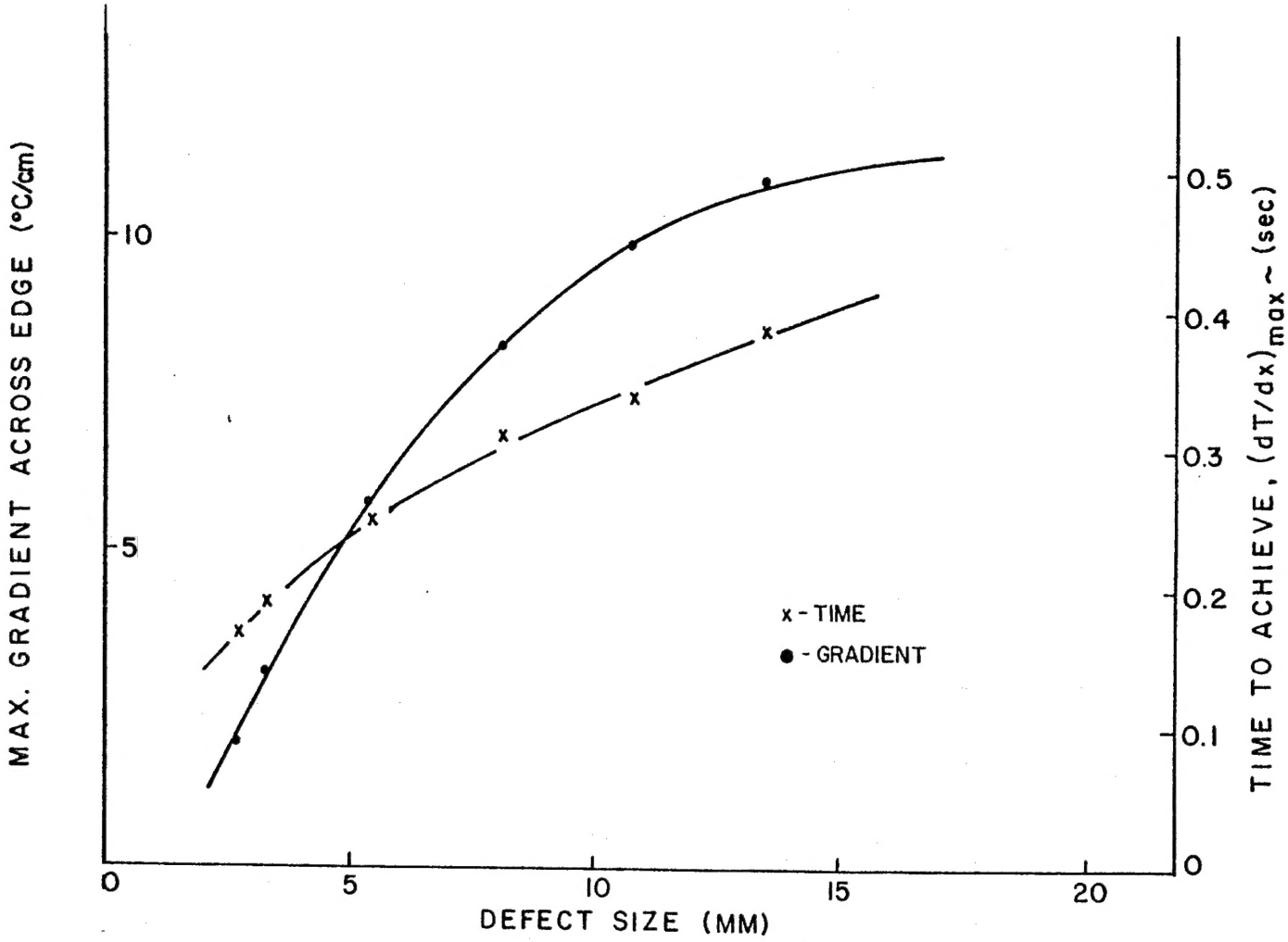

FIGURE 9 . EFFECT OF FLAW DEPTH IN G/E.